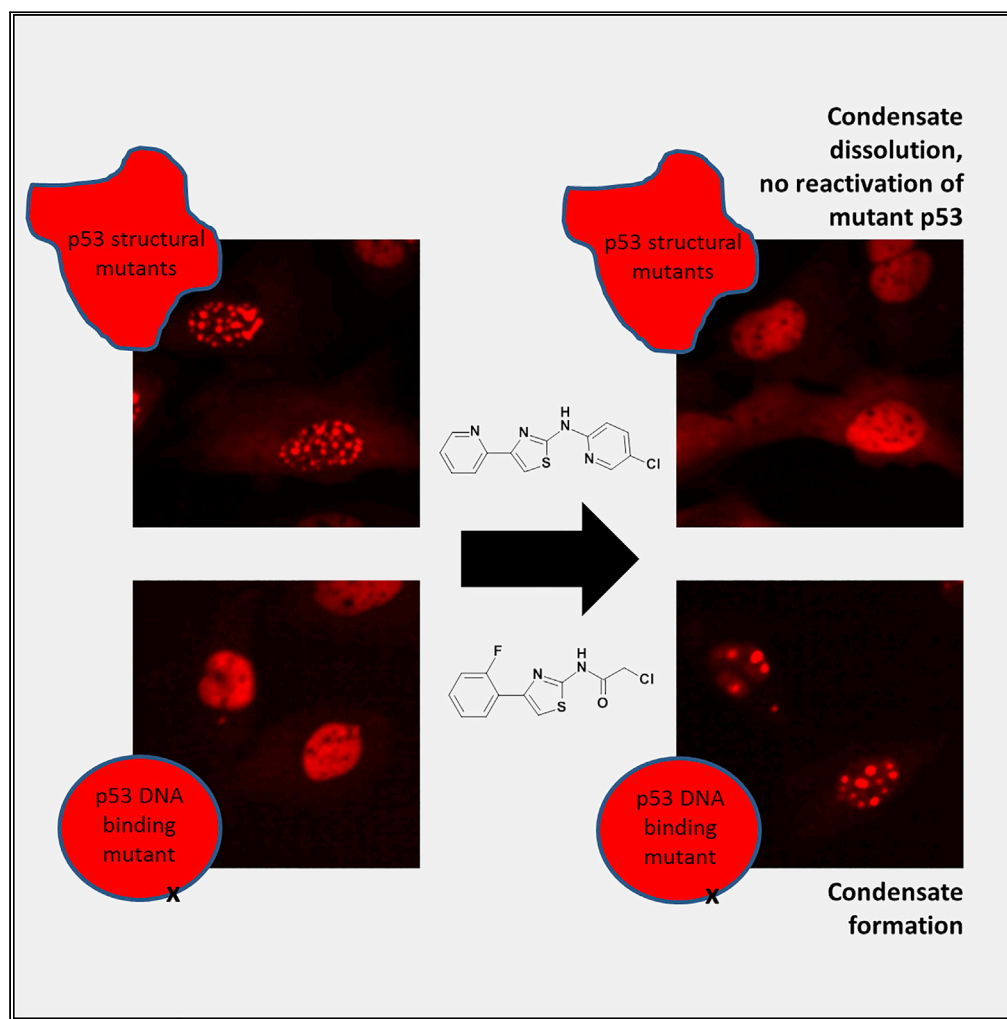


Article

Identification of Small Molecules that Modulate Mutant p53 Condensation



Clara Lemos, Luise Schulze, Joerg Weiske, ..., Knut Eis, Ashley Eheim, Patrick Steigemann

clara.lemos@bayer.com (C.L.)
patrick.steigemann@nuvisan.com (P.S.)

HIGHLIGHTS

Fluorescent versions of structural p53 mutants form protein condensates in cells

We report the identification of p53-interacting small molecules

Identified compounds differentially alter fluorescent mutant p53 condensation behavior

Article

Identification of Small Molecules that Modulate Mutant p53 Condensation

Clara Lemos,^{1,*} Luise Schulze,^{1,2} Joerg Weiske,^{1,2} Hanna Meyer,^{1,2} Nico Braeuer,^{1,2} Naomi Barak,¹ Uwe Eberspächer,¹ Nicolas Werbeck,^{1,2} Carlo Stresemann,^{1,2} Martin Lange,^{1,2} Ralf Lesche,^{1,2} Nina Zablowsky,^{1,2} Katrin Juenemann,^{1,2} Atanas Kamburov,¹ Laura Martina Luh,¹ Thomas Markus Leissing,¹ Jeremie Mortier,¹ Michael Steckel,¹ Holger Steuber,^{1,2} Knut Eis,¹ Ashley Eheim,¹ and Patrick Steigemann^{1,2,3,*}

SUMMARY

Structural mutants of p53 induce global p53 protein destabilization and misfolding, followed by p53 protein aggregation. First evidence indicates that p53 can be part of protein condensates and that p53 aggregation potentially transitions through a condensate-like state. We show condensate-like states of fluorescently labeled structural mutant p53 in the nucleus of living cancer cells. We furthermore identified small molecule compounds that interact with the p53 protein and lead to dissolution of p53 structural mutant condensates. The same compounds lead to condensation of a fluorescently tagged p53 DNA-binding mutant, indicating that the identified compounds differentially alter p53 condensation behavior depending on the type of p53 mutation.

In contrast to p53 aggregation inhibitors, these compounds are active on p53 condensates and do not lead to mutant p53 reactivation. Taken together our study provides evidence for structural mutant p53 condensation in living cells and tools to modulate this process.

INTRODUCTION

The transcription factor p53 integrates diverse cellular stress events and regulates the expression of stress response genes and can induce apoptotic and anti-proliferative processes. As a potent tumor suppressor, p53 is frequently downregulated or mutated in tumors, a state associated with adverse prognosis in cancer (Donehower et al., 2019; Kastenhuber and Lowe, 2017).

Cancer cells can suppress p53 activity via different mechanisms. Cellular p53 levels are kept low by ubiquitin-mediated protein degradation. Accordingly, MDM2 as one of the relevant E3 ligases is characterized as an oncogene and is frequently upregulated in a variety of human cancers (Wang et al., 2017). Compounds that disrupt MDM2-p53 interaction have been identified and profiled for potential anti-cancer therapies in tumors with wild-type p53 (Wang et al., 2017). However, depending on the cancer type a large amount of tumors contain truncating or inactivating p53 mutations that most likely would not positively respond to MDM2-directed therapies. Indeed, most p53 mutations occur as missense mutations in the DNA-binding domain of p53 and result in inactivated transcription factor function, MDM2 insensitivity, and can confer oncogenic gain of function (Donehower et al., 2019; Muller and Vousden 2013, 2014; Soussi and Wiman, 2015). A majority of p53 missense mutants fall into several hotspot codons. These can be subdivided based on their functional consequences on p53 into DNA contact defective mutants (e.g., mutants at residue 273) that directly interfere with p53-DNA interactions and structural mutants that lead to p53 misfolding and aggregation (Donehower et al., 2019; Muller and Vousden 2013, 2014; Rangel et al., 2014; Silva et al., 2014, 2018; Soussi and Wiman, 2015; Xu et al., 2011).

Structural p53 mutants such as R175H, R282W, and Y220C lead to global protein destabilization and protein misfolding. p53 misfolding in turn is thought to lead to the externalization of an aggregation-prone segment followed by prion-like aggregation and inactivation of mutant p53 (Costa et al., 2016; Rangel et al., 2014; Silva et al., 2014, 2018; Soragni et al., 2016; Wang and Fersht, 2017).

¹Bayer AG Research and Development, Pharmaceuticals, Müllerstr. 178, 13342 Berlin, Germany

²Present address: Nuvisan ICB GmbH, Müllerstr. 178, 13342 Berlin, Germany

³Lead Contact

*Correspondence: clara.lemos@bayer.com (C.L.), patrick.steigemann@nuvisan.com (P.S.)

<https://doi.org/10.1016/j.isci.2020.101517>



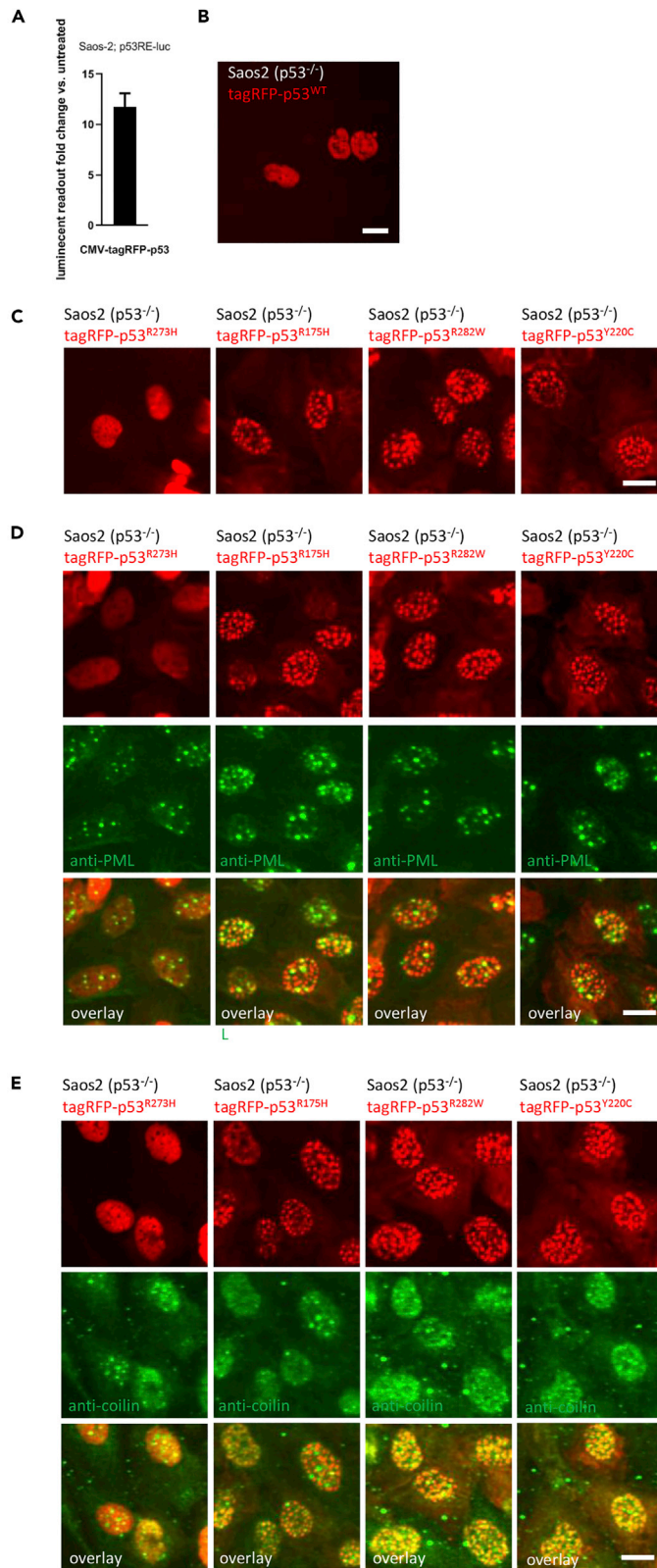


Figure 1. Condensate Formation of Fluorescent Structural Mutant p53 Variants

(A) Saos2 containing a p53 activity reporter showed reporter activation after transduction of a tagRFP-p53 expression vector. Luminescent readout normalized to DMSO controls. Bars show mean with SD (n = 3).
(B) Saos2 cells transiently transfected with a tagRFP-p53^{WT} expression vector show homogeneous distribution of tagRFP-p53 in the nucleus. Scale bar, 10 μ m.
(C) Saos2 cells expressing fluorescently tagged structural mutants show p53 condensates in the nuclei. Scale bars, 10 μ m.
(D and E) Antibody staining of Saos2 cells expressing fluorescently tagged structural mutants with anti-PML or coilin antibodies. No co-localization of fluorescently tagged mutant p53 condensates with either PML (D) or Cajal bodies (E) in the nucleus is observable. Scale bars, 10 μ m.

p53 structural mutants form aggregates that co-aggregate with and inactivate interaction partners such as p53 family members p63 and p73 (Costa et al., 2016; Gaiddon et al., 2001; Liu et al., 2011; Muller and Vousden, 2013; Wiech et al., 2012; Xu et al., 2011). This can explain potential oncogenic gain-of-function effects of p53 structural mutants resulting in the development of more invasive tumor phenotypes and poorer prognosis. Furthermore, structural mutant p53 aggregates show prion-like behavior (Silva et al., 2018). As a significant part of human tumors harbor structural mutant forms of the p53 protein, approaches aimed at preventing mutant p53 gain of function and disrupting the pathological interactions among p53 family members as well as preventing amyloidogenic prion-like properties might be of clinical value (Lang et al., 2004; Li and Prives, 2007; Li et al., 2019; Mantovani et al., 2019; Muller and Vousden 2013, 2014; Olive et al., 2004; Silva et al., 2018; Wang and Fersht, 2017; Xu et al., 2011).

Recent work suggests that p53 potentially transitions through a condensate-like state before aggregation (Boija et al., 2018; Kamagata et al., 2020; Safari et al., 2019; Silva et al., 2018). Here, we show that fluorescently labeled structural p53 mutants, but not DNA-binding defective mutants, form liquid-like condensates in the nucleus of living cancer cells.

Furthermore, we report the identification of small molecules that show direct interaction with p53. In contrast to other structural mutant p53 reactivators (Bykov et al., 2018; Li et al., 2019; Silva et al., 2018), the compounds reported here differentially modulate condensation properties of p53 mutants without leading to mutant p53 reactivation. Therefore the identified small molecules constitute a separate class of p53-directed compounds. These can be used as tool compounds to dissect structural p53 loss-of-function and gain-of-function effects and have the potential to be developed into anti-cancer drugs targeting mutant p53 condensation.

RESULTS**Condensate Formation of Mutant p53 Variants**

To directly monitor condensation or aggregation of p53 in live cells, we established a series of fluorescently labeled (monomeric tagRFP (Merzlyak et al., 2007)) p53 mutant variants expressed in the otherwise p53^{-/-} Saos2 cell line. Transient expression of fluorescently tagged p53^{WT} activated a p53 activity reporter and confirmed general functionality of fluorescently tagged p53 (Figure 1A). As expected, tagRFP-p53^{WT} is homogeneously distributed in the nucleus of Saos2 cells (Figure 1B). According to its role as a tumor suppressor with anti-proliferative activity it was not possible to establish cell lines stably expressing fluorescently labeled p53^{WT}. However, similar to tag-RFP-p53^{WT}, cells stably expressing a fluorescent version of the DNA contact mutant p53^{R273H} showed mainly homogeneous distribution of the fluorescent signal throughout the nucleus (Figure 1C, Video 1D). In stark contrast, stable cell lines expressing fluorescent versions of the structural mutants p53^{R175H} (Figures 1C, Video 1A), p53^{R282W} (Figure 1C, Video 1B), and p53^{Y220C} (Figure 1C, Video 1C) showed dot-like accumulation at several foci throughout the nucleus. Similar condensate-like structures could also be observed in H1299 (p53^{-/-}) and AU565 (p53^{R175H}) cells expressing tagRFP-p53^{R175H} (Figure S1). Protein condensates are characterized by a spherical shape and their ability to fuse (Alberti et al., 2019; Banani et al., 2017; Boija et al., 2018; Cai et al., 2019; Safari et al., 2019; Shin and Brangwynne, 2017). Accordingly, structural mutant tagRFP-p53 foci are spherical and show liquid-like properties and sporadic fusion in live-cell imaging (arrows in Videos 1A, 1B, and 1C). Therefore, based on their condensate-like properties we further refer to the foci as p53 condensates.

To further characterize structural mutant p53 condensates and evaluate if p53 condensates are recruited as clients to preexisting biomolecular nuclear condensates such as promyelocytic leukemia (PML) or Cajal bodies (Ditlev et al., 2018) or exist as independent condensates we stained Saos2 cells expressing

| Compound | nDSF p53 ^{R175H} D°C | nDSF p53 ^{Y220C} D°C | nDSF p53 ^{WT} D°C |
|-------------|-------------------------------|-------------------------------|----------------------------|
| BAY 249716 | 1.0 | 0.6 | 1.2 |
| BAY 1892005 | -0.4 | 1.1 | 0.8 |

Table 1. nDSF: Stabilization upon Compound Binding

nDSF, nano-differential scanning fluorimetry

Exemplary data of multiple experiments are shown ($n \geq 2$). Ligands, that show a ΔT_m greater than six standard deviations from the mean of the control were considered as hit (stabilizer, bold).

fluorescent mutant p53 with anti-PML or anti-coilin antibodies. We find no colocalization of mutant p53 condensates with either PML (Figure 1D) or Cajal bodies (Figure 1E), indicating that nuclear p53 condensates form independent of PML or Cajal bodies.

Identification of Compounds that Interact with p53 Proteins and Their Effects on Mutant p53 Condensates

A previous high throughput screen (HTS) in the laboratory on an internal compound collection exceeding 4 million compounds (Follmann et al., 2019) identified compounds that potentially interact with mutant p53 (data not shown).

To identify compounds from this hit list that directly interact with the p53 protein, selected substances were tested in nano-differential scanning fluorimetry on recombinantly expressed and purified p53 proteins (comprising the p53 DNA-binding domain, see Material and Methods) of structural mutant p53^{R175H} and p53^{Y220C} as well as p53^{WT}. Generally, p53 containing the structural mutations R175H or Y220C showed significantly lower melting temperatures compared with the WT protein (T_m p53^{WT} = 41.6°C \pm 0.01°C, T_m p53^{R175H} = 35.0°C \pm 0.086°C, p53^{Y220C} = 34.7°C \pm 0.02°C), confirming the destabilizing nature of the mutations (Ang et al., 2006). Compounds from a structural cluster of aminothiazoles showed significant stabilization of p53 (Table 1). BAY 249716 showed significant stabilization of all three p53 protein variants, whereas BAY 1892005 showed stabilization of p53^{WT} and p53^{Y220C}, indicating direct interaction with p53. BAY 1892005 contains a reactive head group (Figure 2A) that could be involved in covalent binding to p53. Indeed, by mass spectrometry, we confirmed that BAY 1892005 binds covalently to mutant p53^{R175H} and p53^{Y220C} (Figures 2B and S2). Taken together we conclude that the identified aminothiazoles potentially directly interact with structural p53 mutant proteins.

Compounds that directly bind to and stabilize mutant p53 have the potential to modulate p53 misfolding, condensation, and aggregation (Bykov et al., 2018; Li et al., 2019; Safari et al., 2019; Silva et al., 2018).

To elucidate if aminothiazoles modulate structural mutant p53 condensates, we treated the cells with BAY 249716 or BAY 1892005 and followed mutant p53 by time-lapse imaging (Videos 2A, 2B, 2C, and 2D). We find that the aminothiazoles lead to a rapid dissolution of structural mutant p53 condensates in most cells of the population (Figures 3A and 3B, Videos 2A, 2B, and 2C). In contrast the same compounds lead to the formation of condensates of the DNA-binding defective mutant p53^{R273H} in some cells of the population (Figure 4, Video 2D). Taken together we conclude that aminothiazoles differentially alter fluorescent mutant p53 condensation behavior depending on the type of p53 mutation (structural vs. DNA-binding mutants). To evaluate if the identified compounds selectively target p53 condensates, treated cells were fixed and stained for PML nuclear bodies. These were not affected by compound treatment, indicating that the identified compounds specifically interfere with mutant p53 condensation (data not shown).

Aminothiazoles Lead to Reduction of Nuclear Accumulation of Endogenous Structural p53 Mutants

Depending on mutational status, endogenous p53 can show nuclear accumulation in specific nuclear inclusion bodies (De Smet et al., 2017). To evaluate the compounds in cells with endogenous structural p53 mutants, we stained four different p53^{R175H} mutant cell lines and one p53^{Y220C} mutant cell line by immunofluorescence (IF) using different antibodies directed against p53 (Figures 5 and S3). Structural p53^{R175H} or p53^{Y220C} mutants lead to p53 inactivation, misfolding, aggregation, and accumulation. Accordingly all cell lines showed positive staining for p53 in the nucleus (Figures 5A–5E and S3A–S3E). Furthermore we

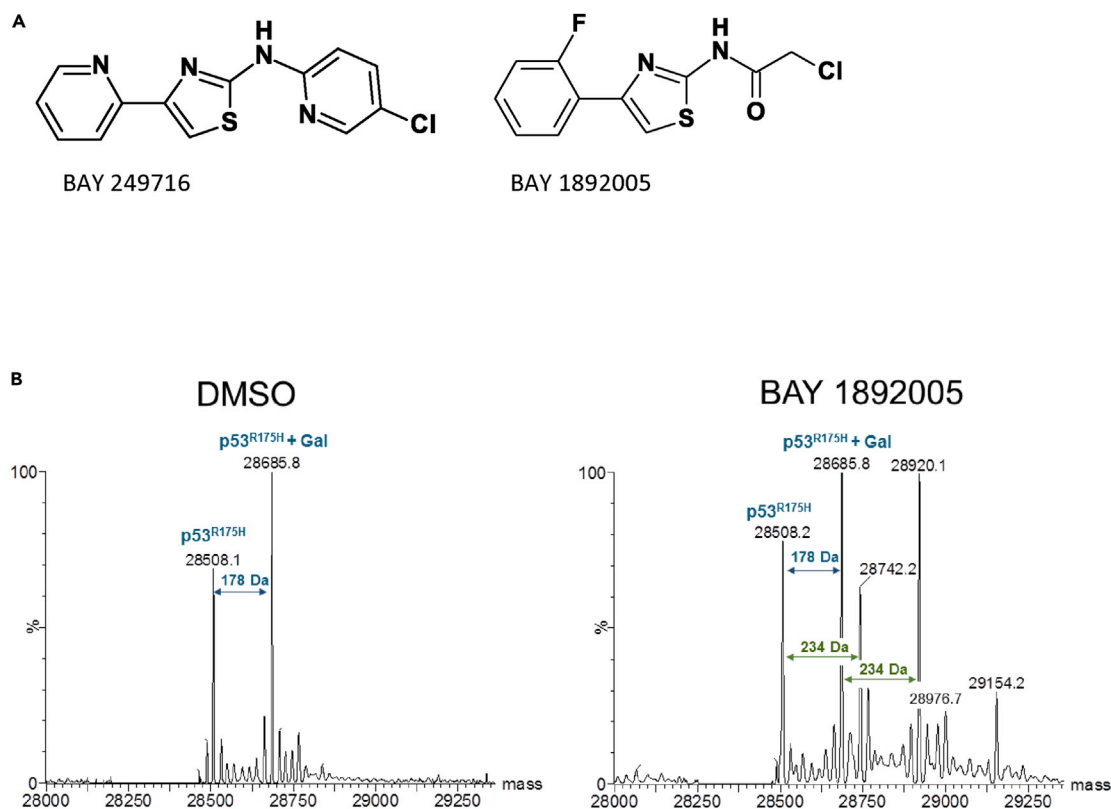


Figure 2. Identification of Compounds that Interact with p53 Proteins

(A and B) (A) Hit compounds. (B) Deconvoluted spectra of intact mass analysis of p53 shows covalent binding of BAY 1892005 to p53^{R175H}. DMSO control shows two peaks of p53^{R175H} protein, one for the expected mass of 28,508 Da and one of 28,685 Da representing N-terminal gluconoylated (Gal) p53^{R175H} (blue arrows). Incubation with BAY 1892005 showed mass shifts of 234 Da to both the apoprotein and the glyconoylated p53^{R175H} (green arrows), indicative for covalent binding of BAY 1892005. An additional mass shift of 234 Da indicates a partial two-fold binding of BAY 1892005 to p53^{R175H}. Exemplary data of multiple experiments are shown ($n \geq 2$).

find a statistically significant reduction in nuclear p53 aggregation in all four cell lines carrying p53^{R175H} after 6 h of aminothiazole treatment (Figures 5A–5D and S3A–S3D). In line with aminothiazoles also binding to p53^{Y220C} (Table 1) and dissolving fluorescent tagRFP-p53^{Y220C} condensates (Figures 3A and B) BAY 249716 also showed a clear reduction of p53 staining intensity in the nucleus of the p53^{Y220C} cell line Huh7 (Figures 5E and S3E). Total p53 protein levels were also evaluated by western blot, in which a slight reduction of total p53 levels was observed (Figure S4). Even though p53 aggregates are present in biopsies and also cell culture cell lines, nuclear p53 aggregates are hard to visualize by IF (De Smet et al., 2017; Pedrote et al., 2020). In line with this, cell lines harboring endogenous structural p53 mutants showed mostly homogeneous staining in the nucleus and no clear visualization of p53 condensates. In addition, we did not find significant changes in antibody stainings after compound treatment with antibodies directed against oligomers or fibrils (data not shown), which indicates that either mutant p53 condensate states do not directly translate into p53 aggregation or as the antibodies are not specific for p53 oligomers or aggregates, they may not be able to resolve subtle changes in oligomeric/amyloid states of p53.

Identified Hits Do Not Lead to Structural Mutant p53 Reactivation

To test for the functional consequence of compound treatment on p53 activity, we generated cell lines containing a p53 response element-driven luciferase reporter (p53 activity reporter, see Material and Methods). Functionality of the reporter was validated in U2OS cells (p53^{WT}) treated with the MDM2 inhibitor Nutlin as well as in Cal-33 (p53^{R175H}) or Saos2 (p53^{-/-}) cells by transduction of a p53 expression vector (Figures 6A–6C).

Next, the compounds were tested for activation of the p53 activity reporter on a set of cell lines with different p53 status. Both aminothiazoles led to weak activation of the p53 activity reporter in Cal-33

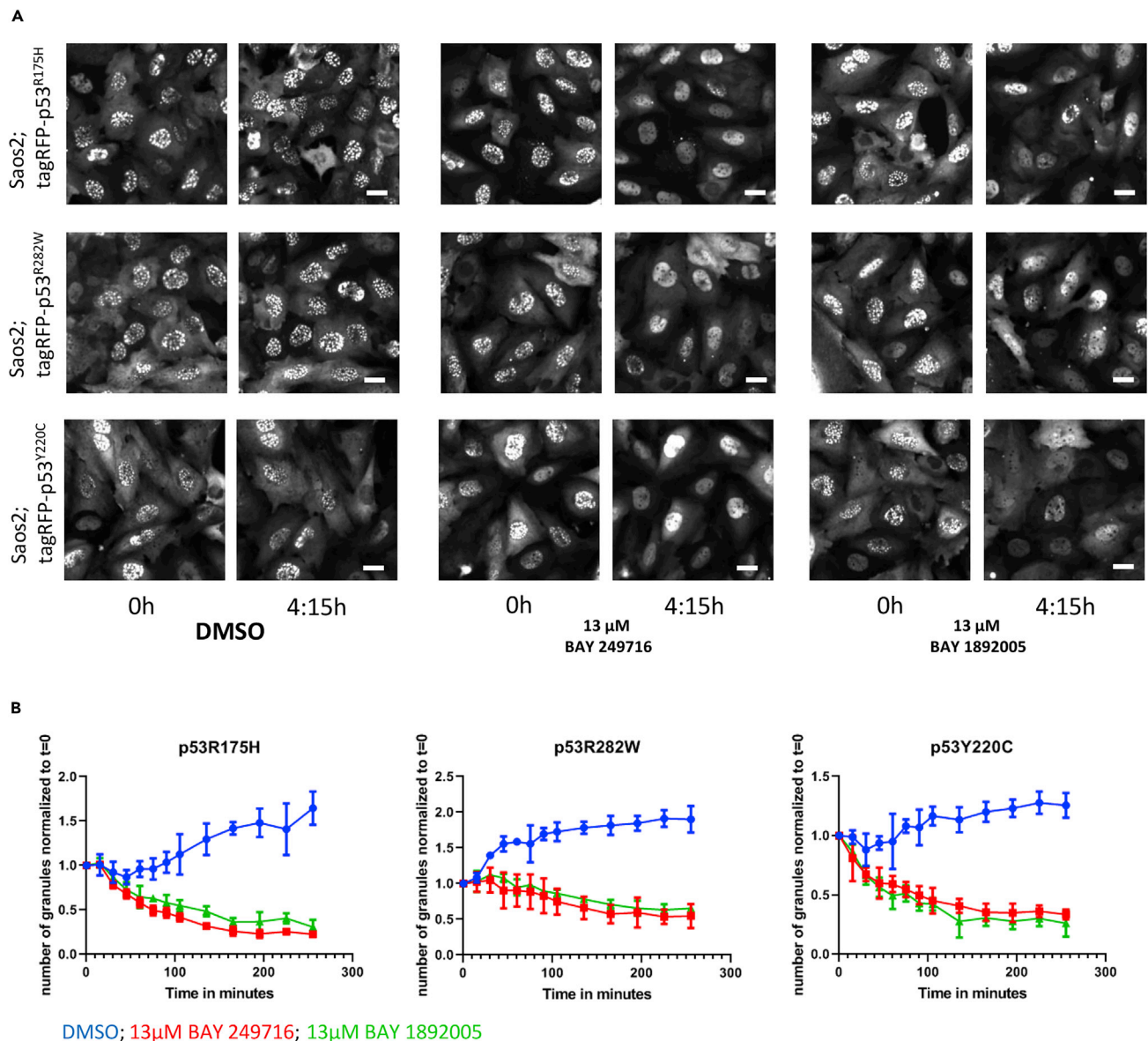


Figure 3. Condensate Formation of Fluorescent Structural Mutant p53 Variants and Their Dissolution by Aminothiazoles

(A) Saos2 cells expressing fluorescently tagged structural mutants show p53 condensates in the nuclei, which are dissolved after aminothiazole treatment. Stills (0 and 4:15 h) from time-lapse Videos 2A, 2B, and 2C. Scale bars, 10 μ m.

(B) Kinetics of condensate dissolution in Saos2 cells expressing structural p53 mutants in response to treatment with aminothiazoles. Bars show mean with SD (n = 4). Exemplary data of multiple experiments are shown (n \geq 2).

and Detroit 562 cells (structural mutant p53^{R175H}), whereas BAY 249716 also showed activity in Huh7 cells (structural mutant p53^{Y220C}) and both showed less activity in MDA-MB-468 cells (DNA contact mutant p53^{R273H}) and in Saos2 or PC3 cells (p53^{-/-}). BAY 249716 also showed p53 activity reporter activation in U2OS cells (p53^{WT}) (Figure 6D), and both compounds showed slight activation of the p53 activity reporter in Calu1 and H358 cells (p53^{-/-}) (Figure 6E). To further elucidate if aminothiazoles lead to the reactivation of structural p53 mutants, we tested if the compounds induce the p53 activity reporter in p53^{-/-} cells stably expressing mutant p53. Treatment with aminothiazoles did not lead to stronger activation of the p53 activity reporter compared with control cells in p53^{-/-} Calu1 cells expressing p53^{R175H} or in p53^{-/-} H358 cells expressing the structural p53 mutants p53^{R175H}, p53^{R282W}, or p53^{Y220C} (Figure 6E) or in Saos2 cells expressing fluorescent versions of mutant p53 (data not shown). This indicates that aminothiazoles do not lead to

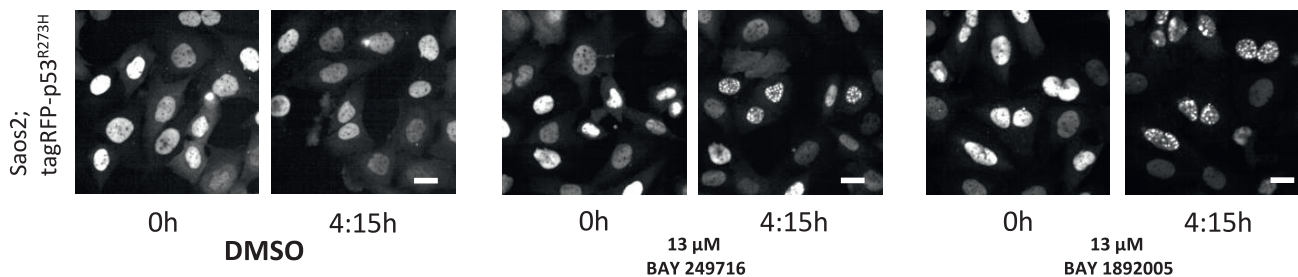


Figure 4. Aminothiazoles Induce Condensation of Fluorescent DNA-Binding Defective p53^{R273H} Mutant Variant

Saos2 cells expressing a fluorescently tagged DNA-binding domain mutant show homogeneous distribution of the fluorescent signal in the nuclei, and aminothiazole treatment leads to the formation of condensate-like structures in some cells of the population. Stills (0 and 4:15 h) from time-lapse [Video 2D](#). Scale bars, 10 μm . Exemplary data of multiple experiments are shown ($n \geq 2$).

reactivation of structural mutant p53 protein. Indeed, p53 knockdown by small interfering RNA in Cal-33 (p53^{R175H}) ([Figure 6F](#)) led to complete loss of nuclear p53 staining but did not prevent activation of the p53 activity reporter ([Figure 6G](#)). Taken together we conclude that aminothiazoles do not lead to direct reactivation of structural p53 mutants.

Structural p53 mutants are thought to show gain of function by co-condensation or co-aggregation of p53^{WT} and other p53 family members such as p73 ([de Oliveira et al., 2015](#); [Kehrloesser et al., 2016](#); [Li and Prives, 2007](#); [Stindt et al., 2015](#)). Therefore, we speculated that the weak p53 activity reporter activation seen in cells with structural p53 mutants could be triggered by activation of p73. Indeed, p53 family members share similar response element structures ([Luh et al., 2013](#)). To test the influence of p73 on p53 reporter activation, we partially knocked down p73 in Cal-33 cells containing the p53 activity reporter ([Figure 6F](#)) and found that reporter activation could be partly suppressed ([Figure 6G](#)). Therefore, we conclude that aminothiazoles act on the p53 activity reporter possibly via p73 activation.

Finally, we tested the aminothiazoles for long-term anti-proliferative activity in a set of cell lines with different p53 mutation status. In summary, we demonstrate that both compounds show anti-proliferative activity independent of p53 status ([Table 2](#)), indicating p53-independent effects of the aminothiazoles on long-term viability.

Taken together we show the visualization of structural mutant p53 condensates in live cells and identify compounds that directly interact with p53 and modulate p53 condensation and nuclear accumulation. As these compounds modulate p53 condensation and do not lead to mutant p53 reactivation, the identified small molecules constitute a separate class of p53-directed compounds.

DISCUSSION

p53 is a transcription factor with a crucial role as a tumor suppressor. p53 controls a wide range of processes including induction of apoptosis and senescence, DNA repair, metabolic and antioxidant responses, and cell-cycle arrest. p53 is inactivated in more than 50% of all cancers. Structural mutants of p53 lead to global p53 protein destabilization ([Ang et al., 2006](#)) and aggregation. Co-aggregation of other p53 family members or other interaction partners could explain specific gain-of-function effects of structural p53 mutants. However, it is unclear how the exact process of p53 aggregation occurs. Recent data indicate that p53 can be organized as part of protein condensates and that p53 aggregation could potentially occur through a transient condensate-like state ([Boija et al., 2018](#); [Kamagata et al., 2020](#); [Kilic et al., 2019](#); [Safari et al., 2019](#)). Using artificial expression of p53 mutants N-terminally tagged with monomeric tagRFP, we show that p53 variants that carry structural mutants p53^{R175H}, p53^{R282W}, or p53^{Y220C} but not the DNA contact mutant p53^{R275H} or p53^{WT} are localized to punctate structures in the nucleus. Given their spherical shape, dynamic behavior during the cell cycle, and fusion events of single spots, these structures potentially represent structural mutant p53 protein condensates ([Alberti et al., 2019](#)). Interestingly, no clearly visible condensate-like structures can be detected in cells with endogenous structural p53 mutants by IF. As condensate-like structures are observed only in cells expressing structural p53 mutants and not in the DNA-binding defective mutant or p53^{WT}, this observation is not an artifact of fluorescent tagging of p53 with monomeric tagRFP but rather a feature of structural p53 mutants. Furthermore, condensate-like

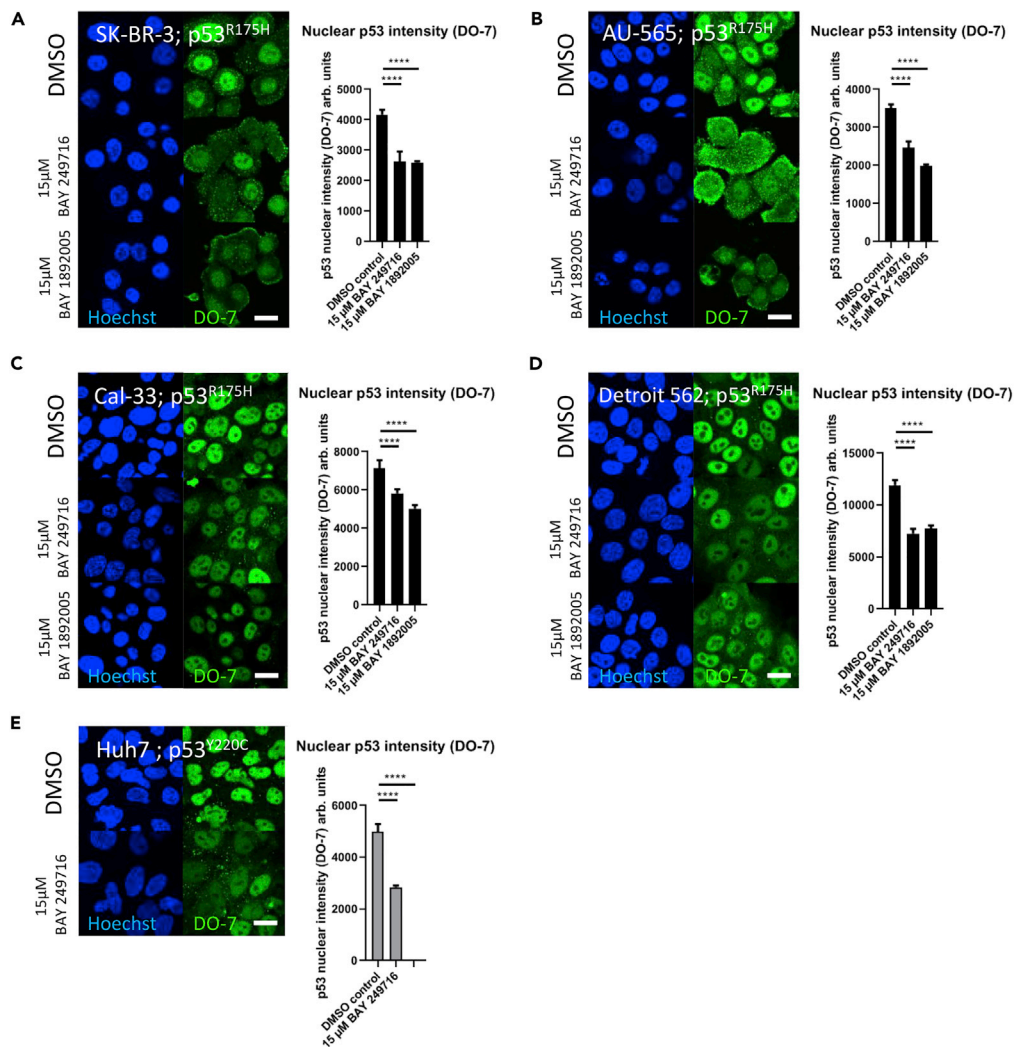


Figure 5. Aminothiazoles Lead to Reduction of Nuclear Accumulation of Endogenous Structural p53 Mutants (A–E) p53^{R175H} cell lines (A) SK-BR-3, (B) AU-565, (C) Cal-33, and (D) Detroit 562 and (E) p53^{Y220C} cell line Huh7 were treated with aminothiazoles for 6 h and stained by IF for p53 (DO-7), and the intensity of the staining in the nucleus was quantified. ****p value < 0.0001. Scale bar, 10 μ m. Bars show mean with SD ($n \geq 5$). Exemplary data of multiple experiments are shown ($n \geq 2$).

structure formation of fluorescently tagged structural p53 mutants is not a cell line-specific effect, as condensate-like structures could also be observed after expression of the fluorescent constructs in H1299 (p53^{-/-}) or AU565 (p53^{R175H}) cell lines. p53 has been shown to form anomalous condensate-like states and to co-condensate with other factors (Boija et al., 2018; Kilic et al., 2019; Safari et al., 2019). Indeed p53 contains several intrinsically disordered regions, which are thought to be driving elements for protein condensation (Anbo et al., 2019; Xue et al., 2013). Therefore, we speculate that artificial expression of fluorescent p53 constructs highlights otherwise sub-microscopic condensates that normally are transient structures in the process of mutant p53 aggregation (de Oliveira et al., 2019; De Smet et al., 2017; Pedrote et al., 2020; Safari et al., 2019). Furthermore, the N-terminal region of p53 is important for p53 aggregation (Kamagata et al., 2020; Melo Dos Santos et al., 2019). Therefore modulation of this region by a fluorescent tag could slow down transitioning through a condensate-like state before aggregation and thereby additionally contributing to highlighting otherwise transient p53 condensate states.

Although several compounds and biomolecules have been identified that reactivate mutant p53 and interfere with p53 aggregation, no compounds have been reported that modulate p53 condensation (Bykov

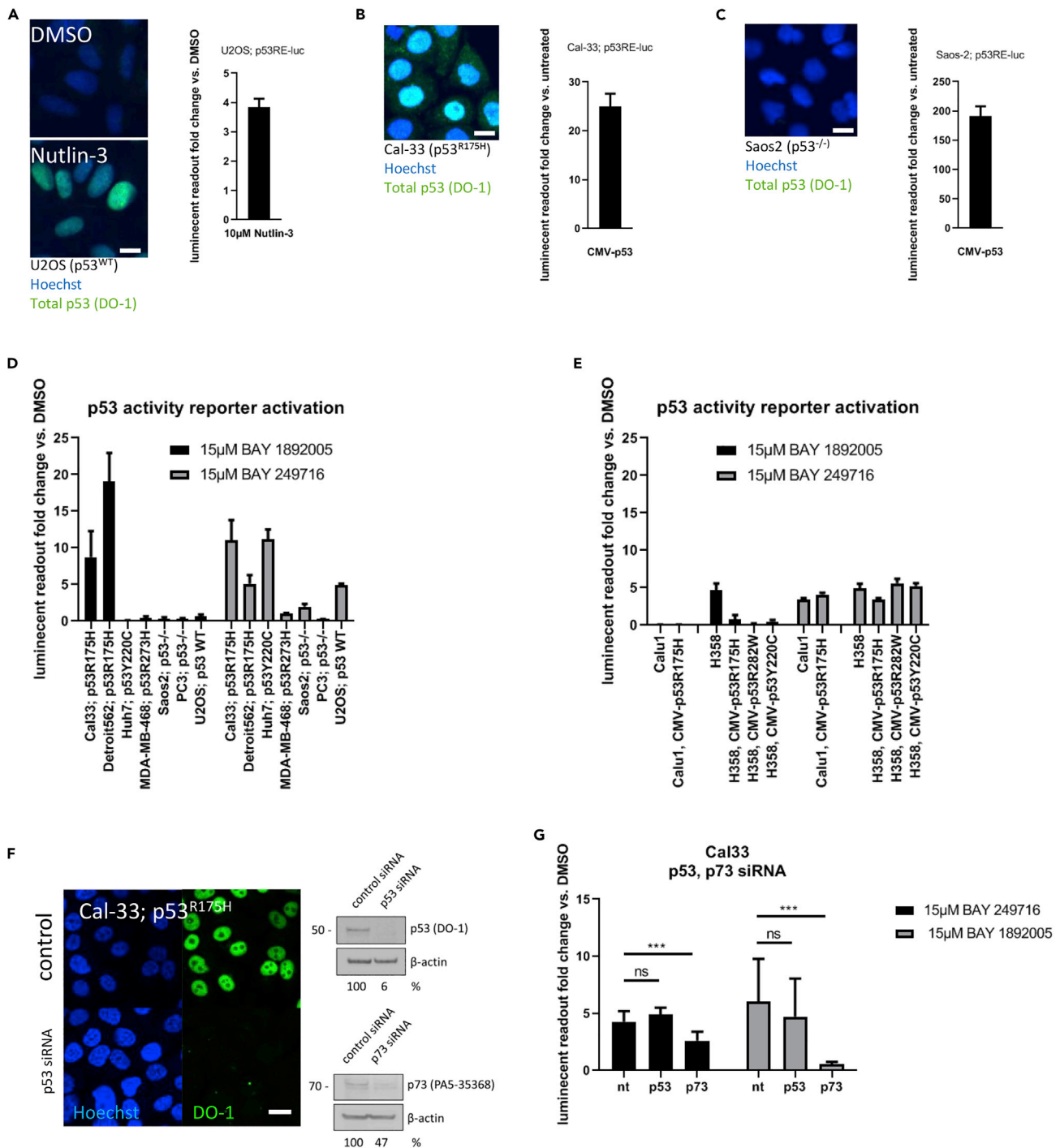


Figure 6. Identified Hits Do Not Lead to Structural Mutant p53 Reactivation

(A) U2OS (p53^{WT}) cells containing the p53 activity reporter show nuclear accumulation of p53 upon 10 μM Nutlin-3 treatment and induction of the activity reporter.

(B) Cal-33 (p53^{R175H}) cells containing the p53 activity reporter show nuclear accumulation of p53^{R175H} and no p53 activity reporter induction after Nutlin-3 treatment (data not shown) but induction after transduction of a CMV-driven p53 expression vector.

(C) Saos2 (p53^{-/-}) cells containing the p53 activity reporter showed no staining for p53 and no induction of the p53 activity reporter after Nutlin-3 treatment (data not shown) but induction of the p53 activity reporter after transduction of a CMV-driven p53 expression vector. Luminescent readout normalized to DMSO controls. Exemplary data of multiple experiments are shown (n ≥ 2) Scale bars, 10 μm.

Figure 6. Continued

- (D) p53 activity reporter activation upon aminothiazole treatment in cells with different p53 mutation status. Luminescent readout normalized to DMSO controls. Exemplary data of multiple experiments are shown ($n \geq 2$), Bars show mean with SD ($n = 8$).
- (E) Expression of structural mutant p53 in p53^{-/-} cells does not enhance p53 activity reporter activation. Luminescent readout normalized to DMSO controls. Exemplary data of multiple experiments are shown ($n \geq 2$), Bars show mean with SD ($n = 8$).
- (F) p53 knockdown validated by IF and western blot; partial p73 knockdown shown in western blot. Exemplary data of multiple experiments are shown ($n \geq 2$); full western blot data show in [Figure S6](#). Scale bar, 10 μm .
- (G) p53 knockdown does not prevent p53 activity reporter activation in Cal-33 cells, whereas p73 knockdown shows suppression of p53 activity reporter activation. Luminescent readout normalized to DMSO controls. Exemplary data of multiple experiments are shown ($n \geq 2$), Bars show mean with SD ($n = 10$). ***p value < 0.001; ns, not significant.

[et al., 2018](#); [Li et al., 2019](#)). Mutant p53 condensation, aggregation, and its associated gain-of-function phenotypes as well as their prion-like properties are increasingly viewed as new opportunities for therapeutic intervention. We here identify two compounds that differentially modulate fluorescent mutant p53 condensation behavior. Even though one of the compounds contains a reactive head group and covalently binds to p53, covalent binding is not required for activity, as BAY 249716 does not contain a reactive group for covalent protein modification. Interestingly, the compounds interfere with fluorescent structural mutant p53 condensation but in cells expressing fluorescent DNA contact mutant p53, the same compounds induce p53 condensation in the nucleus. This indicates that the compounds differently interfere with the dynamic behavior of mutant p53 condensation in structural p53 mutants versus DNA-binding defective p53 mutants.

p53 knockdown leads to near-complete reduction of p53 nuclear staining in cells with structural p53 mutants ([Figure 2C](#)). Therefore, nuclear accumulation of structural mutant p53 requires constant replenishment of newly synthesized protein and interference with the condensation or aggregation process of structural mutant p53 should lead to decrease in p53 nuclear aggregation. Accordingly, we find that the identified compounds lead to a reduction of p53 accumulation in different cancer cells with endogenous p53 structural mutants. However, we noted that aminothiazoles seem to not affect all cells in a population homogeneously ([Figure S5](#), arrows). A possible explanation for this could be that aminothiazoles target a specific condensate state that is modulated by co-condensates and co-factors. Indeed, several factors have been reported to influence p53 aggregation ([Stindt et al., 2015](#); [Wiech et al., 2012](#)) and p53 condensates can co-condensate with other factors ([Boija et al., 2018](#); [Kilic et al., 2019](#)). In future studies, it will be interesting to decipher how cellular parameters such as variations in expression level of p53 itself and modulating co-factors as well as the influence of neighboring cells or the cell cycle phase affect the effectivity of aminothiazoles on p53 condensation of cells in a population.

Structural p53 mutants accumulate as amyloid-like protein aggregates ([Levy et al., 2011](#)) and have the capability to co-aggregate other p53 family members and other transcription factors ([Boija et al., 2018](#); [Kilic et al., 2019](#); [Safari et al., 2019](#); [Wiech et al., 2012](#); [Xu et al., 2011](#)). Indeed, we observed that activation of the p53 activity reporter in cells with structural p53 mutants at least partially depends on p73. Therefore, aminothiazoles could act in part by releasing co-condensed or co-aggregated factors from p53 condensates or aggregates. Furthermore, based on the observation that p53 aggregates can be taken up by surrounding cells and induce further aggregation, p53 is considered to show prion-like properties. It will be interesting to see if by modulating p53 condensation the identified aminothiazoles also influence prion-like effects of p53 mutants. Indeed, 2-aminothiazoles have been proposed as potential leads to treat prion diseases ([Gallardo-Godoy et al., 2011](#)).

Given the long-term p53-independent anti-proliferative effects, the molecules reported here are suitable tool compounds for the evaluation of short-term gain-of-function effects of structural p53 mutants. For evaluation of long-term effects, e.g., on prevention of mutant p53 gain-of-function effects on cell migration or invasion or prion-like effects, optimization of the compounds should separate p53-dependent from additional p53-independent effects.

Limitations of the Study

This study identifies condensation-like states of fluorescent structural mutant p53 and identifies tool compounds that differentially modulate p53 condensation, leading to condensate dissolution in fluorescent structural p53 mutant variants and at the same time inducing condensation of a DNA-binding defective fluorescent p53 variant in a time frame 6 h after compound addition. These compounds do not lead to direct mutant p53 reactivation but seem to activate p53 reporter constructs partially by activation of

| Anti-proli IC50 [M] | p53 ^{R175H} | | | | P53 ^{Y220C} | p53 ^{-/-} | | | | | p53 ^{WT} | |
|------------------------|----------------------------|----------------------------|----------------------------|----------------------------|----------------------------|----------------------------|----------------------------|----------------------------|----------------------------|----------------------------|----------------------------|----------------------------|
| | Cal-33 | Detroit 562 | SK-BR-3 | Au -565 | Huh7 | Saos2 | H1299 | H358 | Calu1 | HMC-1-8 | U2OS | MCF7 |
| BAY 249716 | 1.88 × 10 ⁻⁶ | 1.86 × 10 ⁻⁶ | 2.20 × 10 ⁻⁶ | 6.78 × 10 ⁻⁶ | 7.27 × 10 ⁻⁶ | 4.07 × 10 ⁻⁶ | 2.54 × 10 ⁻⁶ | 7.12 × 10 ⁻⁶ | 2.82 × 10 ⁻⁶ | 7.57 × 10 ⁻⁷ | 4.29 × 10 ⁻⁶ | 8.15 × 10 ⁻⁷ |
| BAY 1892005 | 4.21 × 10 ⁻⁶ | 9.70 × 10 ⁻⁶ | 5.19 × 10 ⁻⁶ | 9.78 × 10 ⁻⁶ | 1.12 × 10 ⁻⁵ | 4.60 × 10 ⁻⁶ | 9.76 × 10 ⁻⁶ | 1.11 × 10 ⁻⁵ | 1.32 × 10 ⁻⁶ | 2.21 × 10 ⁻⁶ | 3.97 × 10 ⁻⁶ | 6.81 × 10 ⁻⁶ |

Table 2. Anti-proliferative IC50 of Compounds Tested on Cell Lines with Different p53 Mutation Status

p73. The identified compounds showed p53-independent anti-proliferative behavior in long-term proliferation experiments, indicating additional p53-independent activities. Therefore optimization of the compounds should separate p53-dependent from additional p53-independent effects.

Resource Availability

Lead Contact

Further information and requests for resources and reagents should be directed to and will be fulfilled by the Lead Contact, Patrick Steigemann (patrick.steigemann@nuvisan.com).

Materials Availability

Plasmids generated in this study can be obtained from sirion Biotech (<https://www.sirion-biotech.com>); there are restrictions to the availability of aminothiazoles due to limited stock amounts.

Data and Code Availability

The published article includes all datasets generated or analyzed during this study.

METHODS

All methods can be found in the accompanying [Transparent Methods supplemental file](#).

SUPPLEMENTAL INFORMATION

Supplemental Information can be found online at <https://doi.org/10.1016/j.isci.2020.101517>.

ACKNOWLEDGMENTS

The authors would like to thank Oliver Beutel, Ann Kwong, and Avinash Patel for helpful discussions.

AUTHOR CONTRIBUTIONS

L.S. and N.Z. generated cell lines, performed luciferase, siRNA, IF, and live cell imaging experiments, P.S. analyzed the data. C.L., C.S., and M.L. performed and analyzed cell proliferation and cell mechanistic assays. H.M. performed and analyzed mass spectrometry experiments. J.W., N.Barak., and U.E. performed and analyzed nDSF data. R.L. and A.K. performed and analyzed deep sequencing experiments. K.J. performed and analyzed western blotting. N.Braeuer. supervised Medicinal Chemistry activities. N.W., L.L., T.M.L., J.M., M.S., H.S., K.E., A.E., and P.S. advised on experiments and analysis. This work was conceptualized by C.L. and P.S. P.S. wrote the original draft, which was reviewed by the entire team. P.S. supervised this work.

DECLARATION OF INTERESTS

All authors are or were employees of Bayer AG.

Received: April 30, 2020

Revised: July 27, 2020

Accepted: August 26, 2020

Published: September 25, 2020

REFERENCES

- Alberti, S., Gladfelder, A., and Mittag, T. (2019). Considerations and challenges in studying liquid-liquid phase separation and biomolecular condensates. *Cell* 176, 419–434.
- Anbo, H., Sato, M., Okoshi, A., and Fukuchi, S. (2019). Functional segments on intrinsically disordered regions in disease-related proteins. *Biomolecules* 9, 88.
- Ang, H.C., Joerger, A.C., Mayer, S., and Fersht, A.R. (2006). Effects of common cancer mutations on stability and DNA binding of full-length p53 compared with isolated core domains. *J. Biol. Chem.* 281, 21934–21941.
- Banani, S.F., Lee, H.O., Hyman, A.A., and Rosen, M.K. (2017). Biomolecular condensates: organizers of cellular biochemistry. *Nat. Rev. Mol. Cell Biol* 18, 285–298.
- Boija, A., Klein, I.A., Sabari, B.R., Dall’Agnese, A., Coffey, E.L., Zamudio, A.V., Li, C.H., Shrinivas, K., Manteiga, J.C., Hannett, N.M., et al. (2018). Transcription factors activate genes through the phase-separation capacity of their activation domains. *Cell* 175, 1842–1855 e16.
- Bykov, V.J.N., Eriksson, S.E., Bianchi, J., and Wiman, K.G. (2018). Targeting mutant p53 for efficient cancer therapy. *Nat. Rev. Cancer* 18, 89–102.
- Cai, D., Feliciano, D., Dong, P., Flores, E., Gruebele, M., Porat-Shliom, N., Sukenik, S., Liu, Z., and Lippincott-Schwartz, J. (2019). Phase separation of YAP reorganizes genome topology for long-term YAP target gene expression. *Nat. Cell Biol.* 21, 1578–1589.
- Costa, D.C., de Oliveira, G.A., Cino, E.A., Soares, I.N., Rangel, L.P., and Silva, J.L. (2016). Aggregation and prion-like properties of misfolded tumor suppressors: is cancer a prion disease? *Cold Spring Harb. Perspect. Biol.* 8, a023614.
- de Oliveira, G.A., Rangel, L.P., Costa, D.C., and Silva, J.L. (2015). Misfolding, aggregation, and disordered segments in c-Abl and p53 in human cancer. *Front Oncol.* 5, 97.
- de Oliveira, G.A.P., Cordeiro, Y., Silva, J.L., and Vieira, T. (2019). Liquid-liquid phase transitions and amyloid aggregation in proteins related to cancer and neurodegenerative diseases. *Adv. Protein Chem. Struct. Biol.* 118, 289–331.
- De Smet, F., Saiz Rubio, M., Hompes, D., Naus, E., De Baets, G., Langenberg, T., Hipp, M.S., Houben, B., Claes, F., Charbonneau, S., et al. (2017). Nuclear inclusion bodies of mutant and wild-type p53 in cancer: a hallmark of p53 inactivation and proteostasis remodelling by p53 aggregation. *J. Pathol.* 242, 24–38.
- Ditlev, J.A., Case, L.B., and Rosen, M.K. (2018). Who’s in and who’s out-compositional control of biomolecular condensates. *J. Mol. Biol.* 430, 4666–4684.
- Donehower, L.A., Soussi, T., Korkut, A., Liu, Y., Schultz, A., Cardenas, M., Li, X., Babur, O., Hsu, T.K., Lichtarge, O., et al. (2019). Integrated analysis of TP53 gene and pathway Alterations in the cancer genome Atlas. *Cell Rep* 28, 1370–1384 e5.
- Follmann, M., Briem, H., Steinmeyer, A., Hillisch, A., Schmitt, M.H., Haning, H., and Meier, H. (2019). An approach towards enhancement of a screening library: the Next Generation Library Initiative (NGLI) at Bayer - against all odds? *Drug Discov. Today* 24, 668–672.
- Gaiddon, C., Lokshin, M., Ahn, J., Zhang, T., and Prives, C. (2001). A subset of tumor-derived mutant forms of p53 down-regulate p63 and p73 through a direct interaction with the p53 core domain. *Mol. Cell Biol* 21, 1874–1887.
- Gallardo-Godoy, A., Gever, J., Fife, K.L., Silber, B.M., Prusiner, S.B., and Renslo, A.R. (2011). 2-Aminothiazoles as therapeutic leads for prion diseases. *J. Med. Chem.* 54, 1010–1021.
- Kamagata, K., Kanbayashi, S., Honda, M., Itoh, Y., Takahashi, H., Kameda, T., Nagatsugi, F., and Takahashi, S. (2020). Liquid-like droplet formation by tumor suppressor p53 induced by multivalent electrostatic interactions between two disordered domains. *Sci. Rep.* 10, 580.
- Kastenhuber, E.R., and Lowe, S.W. (2017). Putting p53 in context. *Cell* 170, 1062–1078.
- Kehrloesser, S., Osterburg, C., Tuppi, M., Schafer, B., Vousden, K.H., and Dotsch, V. (2016). Intrinsic aggregation propensity of the p63 and p73 T1 domains correlates with p53R175H interaction and suggests further significance of aggregation events in the p53 family. *Cell Death Differ* 23, 1952–1960.
- Kilic, S., Lezaja, A., Gatti, M., Bianco, E., Michelena, J., Imhof, R., and Altmeyer, M. (2019). Phase separation of 53BP1 determines liquid-like behavior of DNA repair compartments. *EMBO J.* 38, e101379.
- Lang, G.A., Iwakuma, T., Suh, Y.A., Liu, G., Rao, V.A., Parant, J.M., Valentin-Vega, Y.A., Terzian, T., Caldwell, L.C., Strong, L.C., et al. (2004). Gain of function of a p53 hot spot mutation in a mouse model of Li-Fraumeni syndrome. *Cell* 119, 861–872.
- Levy, C.B., Stumbo, A.C., Ano Bom, A.P., Portari, E.A., Cordeiro, Y., Silva, J.L., and De Moura-Gallo, C.V. (2011). Co-localization of mutant p53 and amyloid-like protein aggregates in breast tumors. *Int. J. Biochem. Cell Biol* 43, 60–64.
- Li, Y., and Prives, C. (2007). Are interactions with p63 and p73 involved in mutant p53 gain of oncogenic function? *Oncogene* 26, 2220–2225.
- Li, Y., Wang, Z., Chen, Y., Petersen, R.B., Zheng, L., and Huang, K. (2019). Salvation of the fallen angel: reactivating mutant p53. *Br. J. Pharmacol.* 176, 817–831.
- Liu, K., Ling, S., and Lin, W.C. (2011). TopBP1 mediates mutant p53 gain of function through NF-Y and p63/p73. *Mol. Cell Biol* 31, 4464–4481.
- Luh, L.M., Kehrloesser, S., Deutsch, G.B., Gebel, J., Coutandin, D., Schafer, B., Agostini, M., Melino, G., and Dotsch, V. (2013). Analysis of the oligomeric state and transactivation potential of TAp73alpha. *Cell Death Differ* 20, 1008–1016.
- Mantovani, F., Collavin, L., and Del Sal, G. (2019). Mutant p53 as a guardian of the cancer cell. *Cell Death Differ* 26, 199–212.
- Melo Dos Santos, N., de Oliveira, G.A.P., Ramos Rocha, M., Pedrote, M.M., Diniz da Silva Ferretti, G., Pereira Rangel, L., Morgado-Diaz, J.A., Silva, J.L., and Rodrigues Pereira Gimba, E. (2019). Loss of the p53 transactivation domain results in high amyloid aggregation of the Delta40p53 isoform in endometrial carcinoma cells. *J. Biol. Chem.* 294, 9430–9439.
- Merzlyak, E.M., Goedhart, J., Shcherbo, D., Bulina, M.E., Shcheglov, A.S., Fradkov, A.F., Gaintzeva, A., Lukyanov, K.A., Lukyanov, S., Gadella, T.W., and Chudakov, D.M. (2007). Bright monomeric red fluorescent protein with an extended fluorescence lifetime. *Nat. Methods* 4, 555–557.
- Muller, P.A., and Vousden, K.H. (2013). p53 mutations in cancer. *Nat. Cell Biol* 15, 2–8.
- Muller, P.A., and Vousden, K.H. (2014). Mutant p53 in cancer: new functions and therapeutic opportunities. *Cancer Cell* 25, 304–317.
- Olive, K.P., Tuveson, D.A., Ruhe, Z.C., Yin, B., Willis, N.A., Bronson, R.T., Crowley, D., and Jacks, T. (2004). Mutant p53 gain of function in two mouse models of Li-Fraumeni syndrome. *Cell* 119, 847–860.
- Pedrote, M.M., Motta, M.F., Ferretti, G.D.S., Norberto, D.R., Spohr, T., Lima, F.R.S., Gratton, E., Silva, J.L., and de Oliveira, G.A.P. (2020). Oncogenic gain of function in glioblastoma is linked to mutant p53 amyloid oligomers. *iScience* 23, 100820.
- Rangel, L.P., Costa, D.C., Vieira, T.C., and Silva, J.L. (2014). The aggregation of mutant p53 produces prion-like properties in cancer. *Prion* 8, 75–84.
- Safari, M.S., Wang, Z., Tailor, K., Kolomeisky, A.B., Conrad, J.C., and Vekilov, P.G. (2019). Anomalous dense liquid condensates host the nucleation of tumor suppressor p53 fibrils. *iScience* 12, 342–355.
- Shin, Y., and Brangwynne, C.P. (2017). Liquid phase condensation in cell physiology and disease. *Science* 357, eaaf4382.
- Silva, J.L., Cino, E.A., Soares, I.N., Ferreira, V.F., and Oliveria, G., A.P. (2018). Targeting the prion-like aggregation of mutant p53 to combat cancer. *Acc. Chem. Res.* 51, 181–190.
- Silva, J.L., De Moura Gallo, C.V., Costa, D.C., and Rangel, L.P. (2014). Prion-like aggregation of mutant p53 in cancer. *Trends Biochem. Sci.* 39, 260–267.

Soragni, A., Janzen, D.M., Johnson, L.M., Lindgren, A.G., Thai-Quynh Nguyen, A., Tiourin, E., Soriaga, A.B., Lu, J., Jiang, L., Faull, K.F., et al. (2016). A designed inhibitor of p53 aggregation rescues p53 tumor suppression in ovarian carcinomas. *Cancer Cell* 29, 90–103.

Soussi, T., and Wiman, K.G. (2015). TP53: an oncogene in disguise. *Cell Death Differ* 22, 1239–1249.

Stindt, M.H., Muller, P.A., Ludwig, R.L., Kehrlouesser, S., Dotsch, V., and Vousden, K.H. (2015). Functional interplay between MDM2, p63/p73 and mutant p53. *Oncogene* 34, 4300–4310.

Wang, G., and Fersht, A.R. (2017). Multisite aggregation of p53 and implications for drug rescue. *Proc. Natl. Acad. Sci. U S A* 114, E2634–E2643.

Wang, S., Zhao, Y., Aguilar, A., Bernard, D., and Yang, C.Y. (2017). Targeting the MDM2-p53 protein-protein interaction for new cancer therapy: progress and challenges. *Cold Spring Harb. Perspect. Med.* 7, a026245.

Wiech, M., Olszewski, M.B., Tracz-Gaszewska, Z., Wawrzynow, B., Zyllicz, M., and Zyllicz, A. (2012). Molecular mechanism of mutant p53

stabilization: the role of HSP70 and MDM2. *PLoS One* 7, e51426.

Xu, J., Reumers, J., Couceiro, J.R., De Smet, F., Gallardo, R., Rudyak, S., Cornelis, A., Rozenski, J., Zwolinska, A., Marine, J.C., et al. (2011). Gain of function of mutant p53 by coaggregation with multiple tumor suppressors. *Nat. Chem. Biol.* 7, 285–295.

Xue, B., Brown, C.J., Dunker, A.K., and Uversky, V.N. (2013). Intrinsically disordered regions of p53 family are highly diversified in evolution. *Biochim. Biophys. Acta* 1834, 725–738.

Supplemental Information

Identification of Small Molecules that Modulate Mutant p53 Condensation

Clara Lemos, Luise Schulze, Joerg Weiske, Hanna Meyer, Nico Braeuer, Naomi Barak, Uwe Eberspächer, Nicolas Werbeck, Carlo Stresemann, Martin Lange, Ralf Lesche, Nina Zablowky, Katrin Juenemann, Atanas Kamburov, Laura Martina Luh, Thomas Markus Leissing, Jeremie Mortier, Michael Steckel, Holger Steuber, Knut Eis, Ashley Eheim, and Patrick Steigemann

Transparent Methods:

Cell culture

All cell lines were obtained from American Type Culture Collection. Cells were cultured in RPMI1640 (Gibco by Thermo Fisher, Waltham, MA, USA). All media were supplemented with 10% fetal calf serum (PAA Laboratories by GE Healthcare, Little Chalfont, UK) and 1% Penicillin/Streptomycin (Sigma-Aldrich, St. Louis, MO, USA). Cells were maintained at 37 °C in a 5% CO₂ and 95% air incubator.

p53 activity reporter cell lines

Based on 13 repeats of the canonical activating p53 response element (Wang et al. 2009)) combined with a minimal CMV promoter a luciferase based p53 activity reporter (13xp53RE-luciferase, please see below for sequence) co-expressing the neomycin resistance gene was generated and transduced via lentivirus into different cell lines containing either p53^{WT} (U2OS), p53^{R175H} (Detroit, Cal-33) , p53^{Y220C} (Huh7), p53^{-/-} (Saos2, Calu1, H358, PC3) or p53^{R273H} (MDA-MB-468). Presence of the p53 activity reporter construct was selected for by adding 500µg/ml Geneticin to the media. The presence of p53 WT in U2OS and p53^{R175H} mutants in Cal-33 and Detroit 562 was confirmed by sequencing (data not shown). Calu1 and H358 cells containing the p53 activity reporter were additionally co-transduced by lentiviral transduction with a CMV driven p53^{R175H} expression construct, H358 cells containing the p53 activity reporter additionally with constructs for the CMV driven expression of p53^{R282W} or p53^{Y220C}. Presence of the mutant p53 expression constructs was selected for by adding 1µg/ml puromycin to the media and expression of mutated p53 was validated by immunofluorescence against p53 (data not shown). Luciferase activity was measured using the luminescence kit Steady-Glo (Promega, Fitchburg,

WI, USA) and a luminescence plate reader (PHERAstar(BMG Labtech, Ortenberg, Germany)) according to the manufacturer's instructions. Briefly, cells were plated at 3000 cells/5 μ l in white 384-well small volume plates (Greiner) using a liquid dispenser (Multidrop Combi, ThermoScientific), 5 μ l compounds were added and cells were either incubated for 16 to 24 h. 5 μ l SteadyGlo(Promega) was then added to cells and incubated for 30 min in the dark. Subsequently, luminescence intensity was measured in a plate reader. Normalization, quality control, and fitting curves for IC₅₀ determination of tested compounds were performed with Genedata Screener® for high-content screening and Genedata Condoseo modules (Genedata AG, Basel, Switzerland).

13xp53RE-luc2 reporter sequence (p53 activity reporter):

ACCACTTTGTACAAGAAAGCTGGGTCTCGAGGGGCATGCCCGGGCATGTCCACGTATGCAGACT
TTACGGGCATGCCCGGGCATGTCCACGTATGCAGACTTTACGGGCATGCCCGGGCATGTCCACG
TATGCAGACTTTACGGGCATGCCCGGGCATGTCCACGTATGCAGACTTTACGGGCATGCCCGGG
CATGTCCACGTATGCAGACTTTACGGGCATGCCCGGGCATGTCCACGTATGCAGACTTTACGGG
CATGCCCGGGCATGTCCACGTATGCAGACTTTACGGGCATGCCCGGGCATGTCCACGTATGCAGACTTTACGGG
TCATATCGGGCATGCCCGGGCATGTCCACGTATGCAGACTTTACGGGCATGCCCGGGCATGTCC
TAGCAGTAGCTCATATCGGGCATGCCCGGGCATGTCCACGTATGCAGACTTTACGGGCATGCCCG
GGGCATGTCCACGTATGCAGACTTTACGGGCATGCCCGGGCATGTCCACGTATGCAGACTTTACGGG
GGTACGGCGTGTACGGTGGGAGGCCTATATAAGCAGAGCTCGTTTGTAGTGAACCGTCAGATCGCTT
AAGGCCACC**ATGGAAGATGCCAAAACATTAAGAAGGGCCCAGCGCCATTCTACCCAC**
TCGAAGACGGGACCGCCGGCGAGCAGCTGCACAAAGCCATGAAGCGCTACGCCCTG
GTGCCCGGCACCATCGCCTTTACCGACGCACATATCGAGGTGGACATTACCTACGCC
GAGTACTTCGAGATGAGCGTTTCGGCTGGCAGAAGCTATGAAGCGCTATGGGCTGAAT
ACAAACCATCGGATCGTGGTGTGCAGCGAGAATAGCTTGCAGTTCTTCATGCCCGTGT
TGGGTGCCCTGTTTCATCGGTGTGGCTGTGGCCCCAGCTAACGACATCTACAACGAGC
GCGAGCTGCTGAACAGCATGGGCATCAGCCAGCCCACCGTCGTATTTCGTGAGCAAGA
AAGGGCTGCAAAGATCCTCAACGTGCAAAGAAGCTACCGATCATAAAAAGATCA
TCATCATGGATAGCAAGACCGACTACCAGGGCTTCAAAGCATGTACACCTTCGTGAC
TTCCATTTGCCACCCGGCTTCAACGAGTACGACTTCGTGCCCGAGAGCTTCGACCGG
GACAAAACCATCGCCCTGATCATGAACAGTAGTGGCAGTACCGGATTGCCCAAGGGC
GTAGCCCTACCGCACCGCACCGCTTGTGTCCGATTAGTCATGCCCGCGACCCCATCT
TCGGCAACCAGATCATCCCCGACACCGCTATCCTCAGCGTGGTGCCATTTACCACG
GCTTCGGCATGTTACCACGCTGGGCTACTTGATCTGCGGCTTTCGGGTGCTGCTCAT
GTACCGCTTCGAGGAGGAGCTATTCTTGCGCAGCTTGCAAGACTATAAGATTCAATCT
GCCCTGCTGGTGCCACACTATTTAGCTTCTTCGCTAAGAGCACTCTCATCGACAAGT
ACGACCTAAGCAACTTGCACGAGATCGCCAGCGGGCGGGGCGCCGCTCAGCAAGGAG
GTAGGTGAGGCCGTGGCCAAACGCTTCCACCTACCAGGCATCCGCCAGGGCTACGG
CCTGACAGAAACAACCAGCGCCATTCTGATCACCCCGAAGGGGACGACAAGCCTG
GCGCAGTAGGCAAGGTGGTGCCCTTCTTCGAGGCTAAGGTGGTGGACTTGGACACCG
GTAAGACACTGGGTGTGAACCAGCGCGGCGAGCTGTGCGTCCGTGGCCCCATGATCA
TGAGCGGCTACGTTAACAACCCCGAGGCTACAAACGCTCTCATCGACAAGGACGGCT
GGCTGCACAGCGGCGACATCGCCTACTGGGACGAGGACGAGCACTTCTTCATCGTGG
ACCGGCTGAAGAGCCTGATCAAATAACAAGGGCTACCAGGTAGCCCCAGCCGAAGT
GAGAGCATCCTGCTGCAACACCCCAACATCTTCGACGCCGGGGTTCGCCGGCCTGCC
GACGACGATGCCGGCGAGCTGCCCGCCGAGTCGTGCTGGAACACGGTAAAAC
CATGACCGAGAAGGAGATCGTGGACTATGTGGCCAGCCAGGTTACAACCGCCAAGAA
GCTGCGCGGTGGTGTTCGTGGACGAGGTGCCTAAAGGACTGACCGGCAAGTT
GGACGCCCGCAAGATCCGCGAGATTCTCATTAAAGGCCAAGAAGGGCGGCAAGATCG
CCGTGAAT TCTCACGGCTTCCCTCCCGAGGTGGAGGAGCAGGCCGCCGGCACCCCTGC
CCATGAGCTGCGCCAGGAGAGCGGCATGGATAGACACCCTGCTGCTTGCGCCAGCG
CCAGGATCAACGTCTAA

13 repeats of a p53 response element

Luc2 coding region

hPEST coding region

Wang, B., Xiao, Z. and Ren, E. C. (2009) Redefining the p53 response element. *Proc Natl Acad Sci U S A*, 106(34), pp. 14373-8.

Fluorescent mutant p53 cell lines

Fluorescent mutant p53 expression vectors were generated (Sirion Biotech, please see below for sequence) and transduced via lentivirus into Saos2 cells. Presence of the mutant p53 expression constructs was selected for by adding 1 µg/ml puromycin to the media. Imaging was performed using a Phenix confocal spinning disc microscope system (PerkinElmer, Waltham, MA, USA) with a 20x or 40x air objective. Image analysis and quantification was performed using Harmony (PerkinElmer, Waltham, MA, USA) or custom written scripts on MetaXpress (Molecular Devices, Sunnyvale, CA, USA).

Fluorescent mutant p53 constructs:

tagRFP-p53, same architecture for all p53 point mutants

```
ATGGTTTCCAAGGGCGAAGAAGCTGATCAAAGAAAACATGCACATGAAGCTGTACATGGAAGGC
ACCGTGAACAACCACCACTTCAAGTGCACCAGCGAAGGCGAGGGCAAGCCTTATGAGGGCAC
CCAGACCATGCGGATCAAGGTGGTGGAAAGTGGCCCTCTGCCTTTCGCCTTTGATATCCTGGC
CACCAGCTTTATGTACGGCAGCCGGACCTTCATCAATCACACCCAGGGCATCCCCGATTTCTTC
AAGCAGAGCTTCCCCGAGGGCTTCACCTGGGAGAGAGTGACCACATACGAGGATGGCGGCGT
GCTGACAGCCACACAGGATACAAGTCTGCAGGACGGCTGCCTGATCTACAACGTGAAGATCCG
GGGCGTGAACCTCCCCAGCAATGGCCCCGTGATGCAGAAGAAAACCCTCGGCTGGGAAGCCA
ACACCGAGATGCTGTATCCTGCCGATGGTGGACTGGAAGGCAGATCCGATATGGCCCTGAAGC
TCGTTGGCGGGACACCTGATCTGCAACTTCAAGACCACCTACAGAAGCAAGAAGCCCGCCA
AGAACCTGAAGATGCCCGGCGTGTACTACGTGGACCACCGGCTGGAAAGAATCAAAGAGGCC
GACAAAGAGACATACGTGAGCAGCACGAAGTGGCCGTGGCCAGATACTGTGACCTGCCTTCT
AAGCTGGGCCACAAGCTGAACAGCGGCTGAGATCTGGATCTGGCGGAGGATCTGCTTCTGG
CGGCTCTGGCTCTATGGAAGAACCCAGAGCGACCCCTCTGTGGAACCTCCTCTGAGCCAAGA
GACATTCAGCGACCTGTGGAAGCTGCTGCCCGAGAACAATGTGCTGAGCCACTGCCTAGCCA
GGCCATGGATGATCTGATGCTGTCCCCTGACGACATCGAGCAGTGGTTCACCGAGGATCCCGG
ACCTGATGAGGCCCTAGAATGCCTGAAGCTGCTCCTCCTGTTGCTCCCGCTCCTGCTGCTCCT
ACACCAGCTGCTCCAGCTCCAGCACCTTCTTGGCCTCTGTCTAGCAGCGTGCCAGCCAGAAA
ACATACCAGGGCAGCTACGGCTTCCGGCTGGGCTTTCTGCATTCTGGCACAGCCAAGAGCGTG
ACCTGCACATACAGCCCCGCTCTGAACAAGATGTTCTGTGAGCTGGCCAAGACATGCCCGTG
CAGCTGTGGGTTGACAGCACACCTCCACCTGGCACAAGAGTCAGAGCCATGGCCATCTACAAG
CAGTCCCAGCACATGACCGAGGTGCTGCGGAGATGTCCTCACCACGAGAGATGCAGCGATAG
CGACGGACTGGCTCCTCCTCAGCACCTGATTAGAGTGGAAAGGCAACCTGAGAGTGGAAATACCT
GGACGACCGGAACACCTTCAGACACAGCGTGGTGGTGCCTTACGAGCCTCCTGAAGTGGGCA
GCGATTGCACCACCATCCACTACAACACTACATGTGCAACAGCAGCTGCATGGGCGGCATGAACA
GAAGGCCATCCTGACCATCATCACCTGGAAGATAGCAGCGGCAACCTGCTGGGCAGAAAC
AGCTTCGAAGTCCGCGTGTGTGCCTGTCTGGCAGAGACAGAAGAACCAGGAAGAGAACCT
GCGGAAGAAGGGCGAGCCACACCACGAACCTTCCACCAGGCAGCACCAAAAGAGCCCTGCCTA
ACAACACCAGCAGCAGCCCTCAGCCTAAGAAGAAGCCTCTGGACGGCGAGTACTTCACACTG
CAGATTCGGGGCAGAGAACGCTTTGAGATGTTTCAGAGAGCTGAACGAGGCCCTGGAAGTAA
GGATGCCAGGCCGGAAAAGAGCCTGGCGGATCTAGAGCCCACAGCAGCCACCTGAAGTCCA
AGAAGGGCCAGAGCACCAGCCGGCACAAGAACTGATGTTCAAGACAGAGGGCCCCGACAG
CGACTGA
```

tagRFP sequence
linker sequence
p53 sequence

Immunofluorescence

After formaldehyde fixation with 4% PFA, cells were permeabilized with 0.1% Triton-X100 (Sigma-Aldrich) and unspecific binding sites were blocked using 1% BSA. Mouse anti-human p53 (DO-1, Thermo Scientific; DO-7, BD Biosciences), anti-PML (abcam ab179466), anti-Coilin (abcam ab87913) were used as primary antibodies and appropriate secondary antibodies conjugated with Alexa-Fluor 488 (Jackson ImmunoResearch) were used. Cell nuclei were stained with Hoechst 33342 (Life Technologies). Images were acquired by an Opera or Phenix confocal spinning disc microscope system (PerkinElmer, Waltham, MA, USA) with a 20x or 40x water objective. Quantification was carried out with the Harmony (PerkinElmer, Waltham, MA, USA) or MetaXpress software (Molecular Devices).

siRNA

To generate gene knockdown cells, Cal-33 cells were incubated with 10 nM siRNA and Lipofectamine RNAiMAX (Thermo Fisher, Waltham, MA, USA, 1:1000) or control (lipid only) in 12- or 384-well plates and incubated for 2 days at 37 °C and 21% O₂. p53 and p73 siRNA were purchased from Dharmacon (ON-Targetplus SMARTpool Human TP53) and (ON-Targetplus SMARTpool Human TP73).

Protein production

P53 wild type (S94-T312) and two mutants (construct Y220C and R175H) were cloned into a vector for His-tagged overexpression in *Escherichia coli*. Proteins were expressed in BL21(DE3) cells following IPTG induction at 17°C. For purification cell pellets were thawed and resuspended in buffer A (20 mM TRIS pH 7.4, 100 mM NaCl, 10 mM Imidazole, 2 mM DTT, 5% glycerol and Complete Inhibitor plus Benzonase). Cells were lysed using Microfluidizer and the cell debris pelleted by

centrifugation. Lysates were applied to a Ni-NTA washed with two column volumes of wash buffer A and eluted with the buffer A plus 300 mM imidazole. A final protein purification was performed by size exclusion chromatography using HiLoad 35/600 Superdex 75 column at 1ml/min in buffer A without imidazole/complete inhibitor collecting the monomeric peak.

nDSF

Thermal melting experiments were carried out using a Prometheus NT.48 instrument (NanoTemper Technologies). Proteins were prepared in 20 mM Tris-HCl pH 7.4, 100 mM NaCl, 5 % Glycerol, 2 mM DTT and 0.5 mg/mL was used as a final concentration in 50 μ L volume. For binding experiments, ligands were added to the mixture at a final concentration of 100 μ M, 1% DMSO was used as control. Compounds were tested in triplicates. The temperature gradient was 2 $^{\circ}$ C per min from 20 to 90 $^{\circ}$ C. The intrinsic protein fluorescence at 330 and 350 nm was recorded. Data were analyzed using Prometheus NT.48 software. Ligands, which show a $+\Delta T_m$ greater than six standard deviations from the mean of the control, were considered as hit (stabilizer).

Western blot analysis

For SDS-PAGE and subsequent western blotting cells were harvested in 1x RIPA lysis buffer supplemented with complete mini protease inhibitor cocktail (Roche). After the total protein concentration was determined with a Bradford protein assay, total cell lysates were boiled for 10 min at 99 $^{\circ}$ C with 1x sample loading buffer and loaded onto a 4-12% SDS-PAGE gel. For immunoblotting proteins were transferred to a nitrocellulose membrane (0.2 μ m pore size, Schleicher & Schuell) and blocked with 5 % milk, incubated with primary antibodies anti-p53 (1:500, ThermoFisher Scientific, DO-1), anti-p73 (1:500, ThermoFisher Scientific, PA5-35368) and anti- β -actin (1:1000, Cell Signaling, #4967), and subsequently incubated

with secondary antibodies IRDye 680 or IRDye 800 (1:10,000; LI-COR Biosciences). Infrared signal was detected using the Odyssey imaging system (Licor).

Intact mass analysis:

25 μ M of p53H175R and p53Y220C protein were incubated with 100 μ M BAY 1892005. Compound dilution were done in sodium acetate from a 10 mM stock solution in DMSO resulting in a final DMSO concentration of 1 %. Reaction were stopped after 1 h via adding 2 μ l of 4 % TFA to 20 μ l reaction volume.

Samples were analysed on a Waters nanoAcquity coupled to a Waters SYNAPT G2-S with ESI source. The Waters nanoAcquity were equipped with a Waters Mass Prep C4, 2.1 x 5mm to desalt the samples. The nanoAcquity settings was as followed: Temperature; 65 °C, flow rate; 100 μ L /min, buffer A; water / 0.1 % formic acid, buffer B; ACN / 0.1 % formic acid, run time; 6 min, gradient: in 3 min from 20% buffer B to 80%.

The Waters SYNAPT G2-S were operating in ESI positive mode with the following settings: Source temperature; 80 °C, desolvation temperature; 150 °C with a desolvation gas flow rate of 500 L/hour, capillary voltage; 3 kV and cone voltage; 40V. The mass data was collected at a range of 150 m/z – 2200 m/z. Raw data were deconvoluted using MaxEnt1 from Waters.

Cell proliferation assays

Cell viability was determined by means of the AlamarBlue® reagent (Thermo Fisher Scientific) in a Victor X3 Multilabel Plate Reader (Perkin Elmer). The Cal-33 (German Collection of Microorganisms and Cell Cultures GmbH (DSMZ)), Detroit 562 (American Type Culture Collection (ATCC)), Huh7 (Japanese Collection of Research Bioresources Cell Bank (JCRB)), Saos2 (DSMZ), H1299 (ATCC), Calu1 (CLS Cell

Lines Service), HMC-1-8 (JCRB), U2OS (ATCC), were seeded at a concentration of 4000 cells/well in 100 μ l of growth medium (RPMI1640, 20% FCS) on 96-well microtiter plates. The SK-BR-3, Au-565, H358 and MCF7 (all from ATCC), were seeded at a concentration of 5000 cells/well in 100 μ l of growth medium (RPMI1640, 20% FCS) on 96-well microtiter plates. The plates were treated with various substance dilutions (3E-5 M, 1E-5 M, 3E-6 M, 1E-6 M, 3E-7 M, 1E-7 M, 3E-8 M, 1E-8 M) and incubated at 37°C for 96 hours. The IC50 values (substance concentration needed for 50% inhibition of cell proliferation) were calculated from fluorescence values of treated vs. untreated cells.

Supplemental Data:

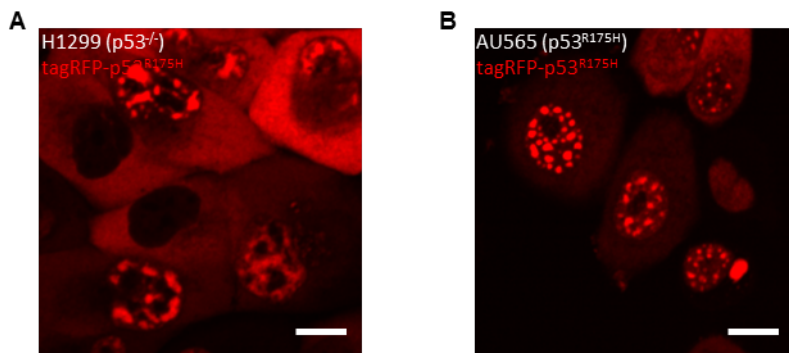


Figure S1: fluorescent p53 reporter, related to Figure 1

A) H1299 and B) AU565 cells expressing fluorescently tagged structural mutant p53^{R175H} show condensate-like structures in the nuclei. Scale bars = 10 μ m

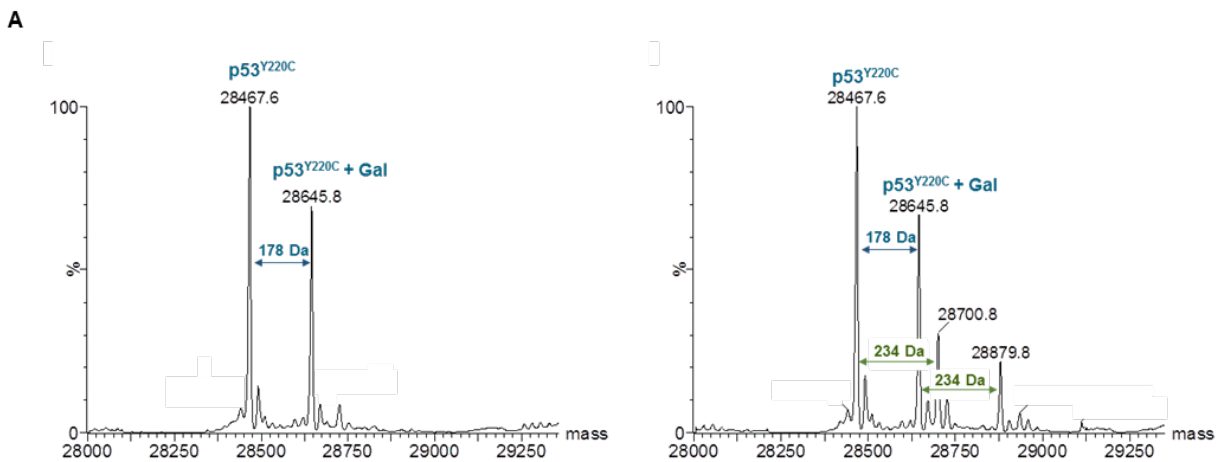


Figure S2: Deconvoluted spectra of intact mass analysis of p53 shows covalent binding of BAY 1892005 to p53^{Y220C}, related to Figure 2. DMSO control shows two peaks of p53^{Y220C} protein, one for the expected mass of 28508 Da and one of 28685 Da representing N-term gluconoylated (Gal) p53^{Y220C} (blue arrows). Incubation with BAY 1892005 showed mass shifts of 234 Da to both the apoprotein and the glyconoylated p53^{Y220C} (green arrows), indicative for covalent binding of BAY 1892005. An additional mass shift of 234 Da indicates a partial two fold binding of BAY 1892005 to p53^{Y220C}.

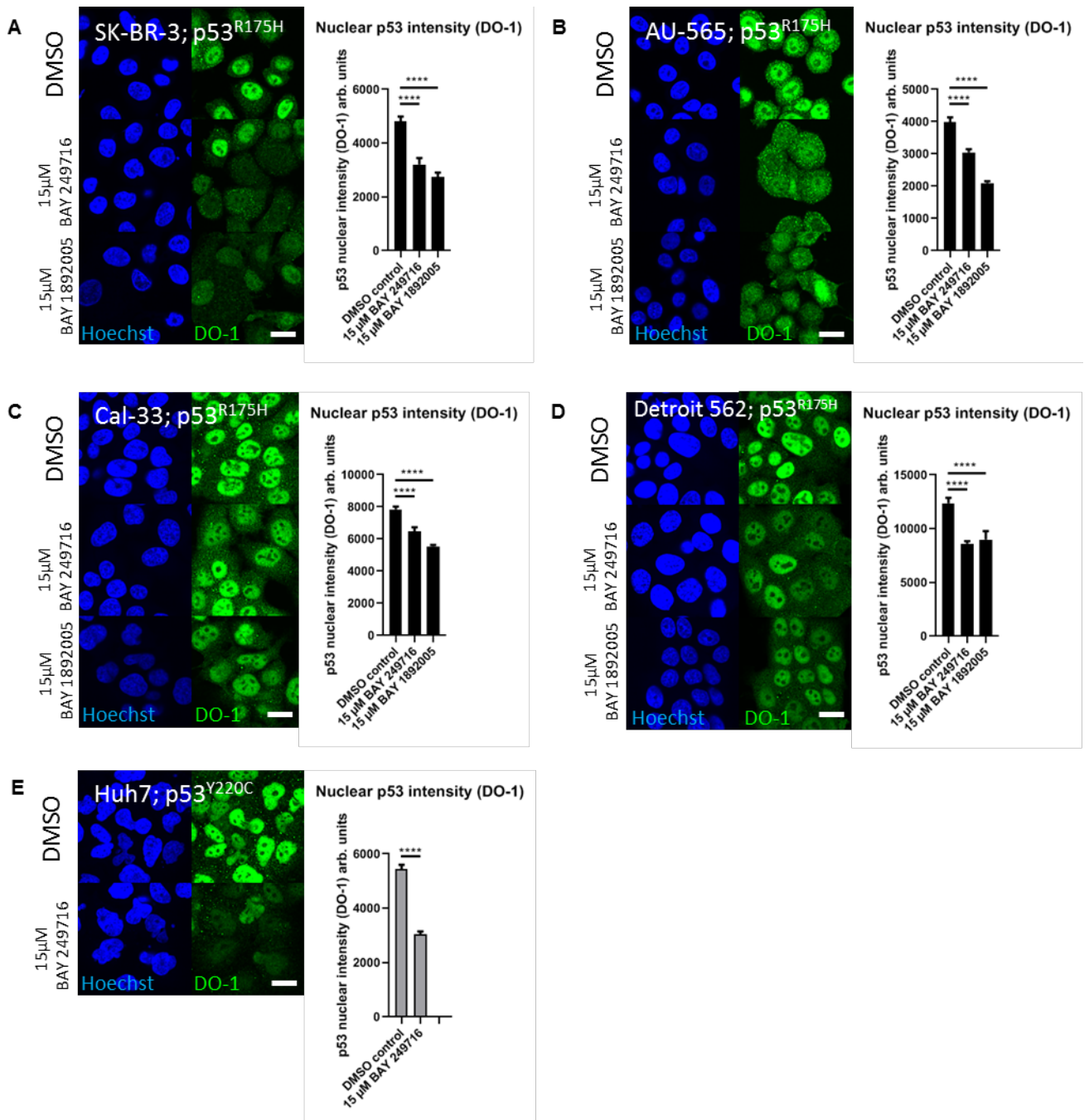


Figure S3: Aminothiazoles lead to reduction of nuclear accumulation of endogenous structural p53 mutants, related to Figure 5

p53^{R175H} cell lines A) SK-BR-3 B) AU-565 C) Cal-33 D) Detroit 562 and E) p53^{Y220C} cell line Huh7 were stained by IF for p53 (DO-1) and the intensity of the staining in the nucleus was quantified. ****p-value < 0.0001. Scale bar = 10μm. Bars show mean with SD (n≥5). Exemplary data of multiple experiments are shown (n ≥ 2).

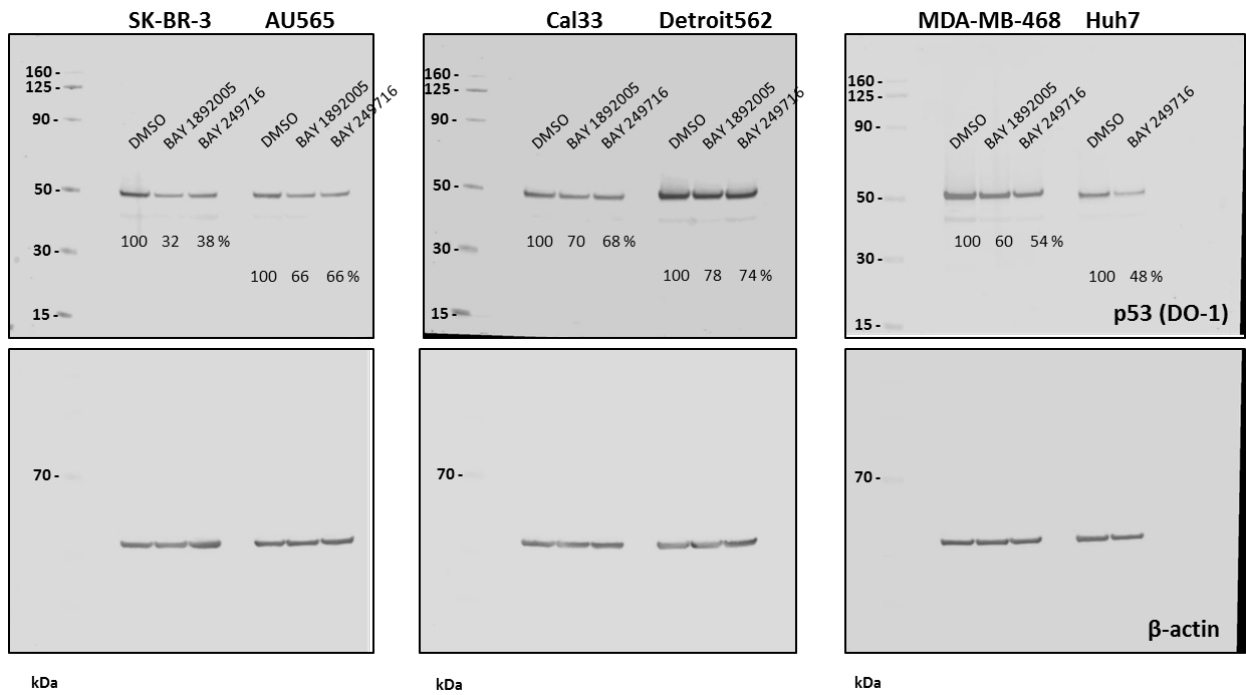


Figure S4: Western Blot quantification shows slight reduction of protein levels in different cell lines after compound treatment, related to Figure 5

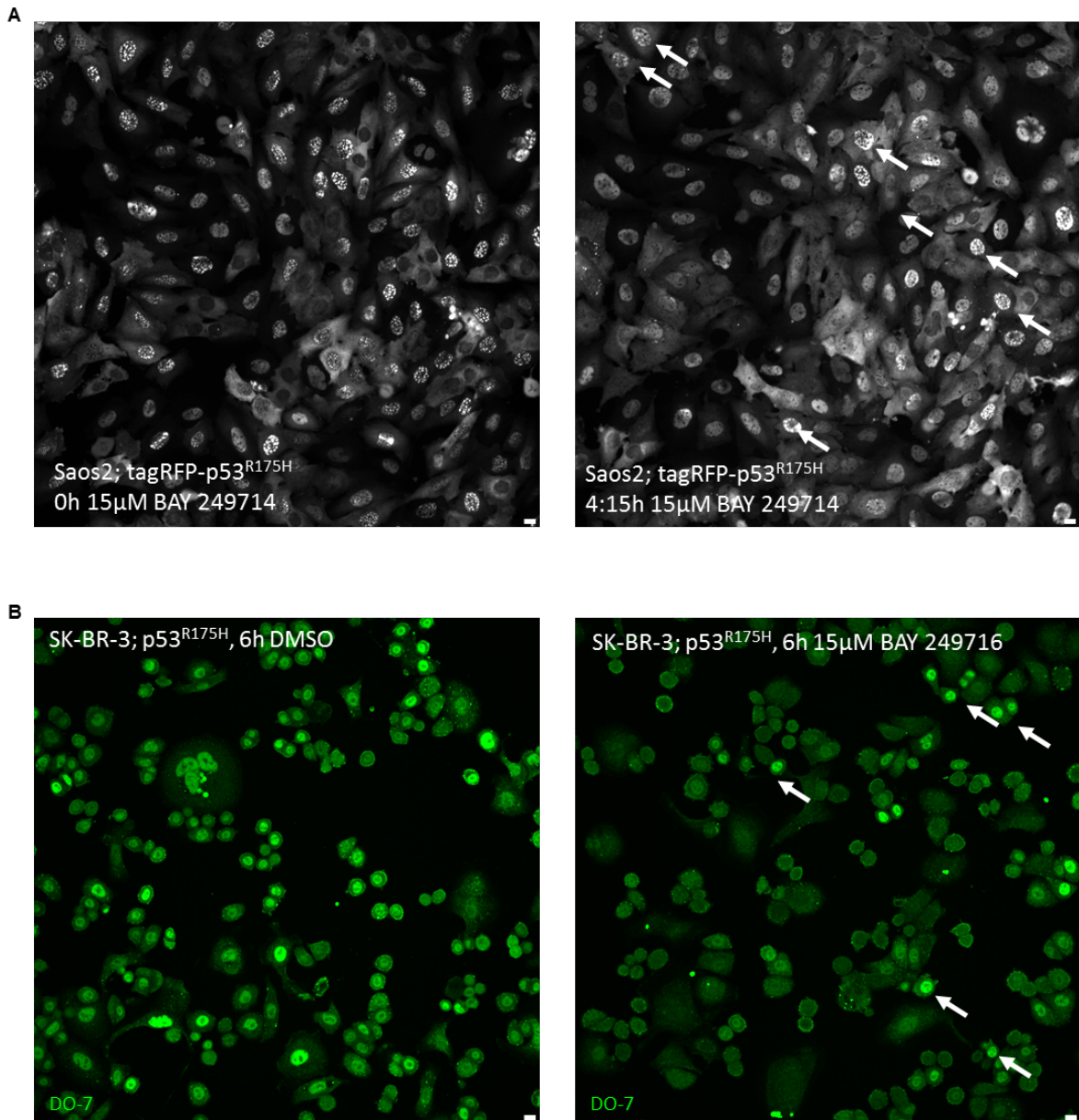
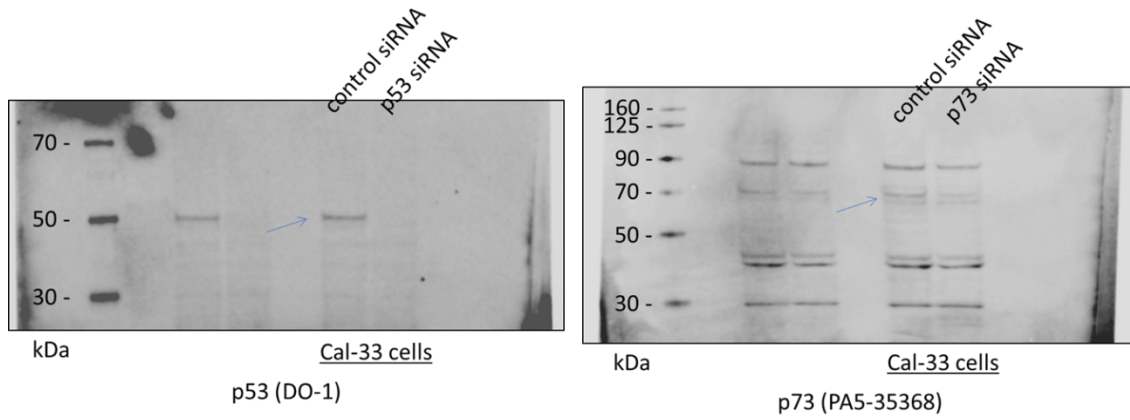


Figure S5: Effect of aminothiazole on cell subpopulations, related to Figure 3 and discussion

A) Saos-2 cells expressing fluorescently tagged structural mutants show p53 condensates in the nuclei which are dissolved after compound treatment with BAY 249716. The overview shows cells displaying dissolution of structural mutant p53 condensates in most cells, while others show less response (arrows). B) SK-BR-3 cells (p53^{R175H}) show a decrease in nuclear staining for endogenous p53 accumulation in the nucleus after treatment with BAY 249716, some cells show less reduction (arrows). Scale bars = 10μm. Exemplary data of multiple experiments are shown ($n \geq 2$).



Figure

Figure S6: Western Blot after p53 or p73 siRNA. Related to Figure 6.